Investigation of Adsorbate Reactivity during NO Decomposition over Different Levels of Copper Ion-Exchanged ZSM-5 Using in Situ IR Technique

Mahesh V. Konduru and Steven S. C. Chuang*

Department of Chemical Engineering, The University of Akron, Akron, Ohio 44325-3906

Received: October 21, 1998; In Final Form: March 23, 1999

In situ infrared (IR) and mass spectroscopy (MS) coupled with temperature-programmed reaction (TPR), isotopic temperature-programmed desorption (TPD), step transient, and pulse transient techniques have been used to study the dynamic behavior of adsorbed species in the NO decomposition reaction on over- and underexchanged Cu−ZSM-5. Overexchanged Cu−ZSM-5 showed higher NO decomposition activity and produced more Cu^+ sites at lower temperatures than the underexchanged sample during the TPR study. Furthermore, overexchanged Cu−ZSM-5 allows rapid equilibrium between gaseous NO and $Cu^+(NO)/Cu^{2+}(NO_3^-)$ during NO decomposition. N_2 formation accompanied by the presence of $Cu^+(NO)$ suggests that Cu^+ initiates the NO decomposition process. However, no direct correlation between $Cu^+(NO)/Cu^+(NO)_2$ intensity and N_2 formation was observed. Adsorbed oxygen from dissociated NO changes the oxidation state of Cu^+ ion, causing the formation of $Cu^{2+}(NO_3^-)$. While $Cu^{2+}(NO_3^-)$ decomposes to N_2, N_2O, NO_2, and O_2 during TPD, it is only partially responsible for the formation of O_2 during NO decomposition. Isotopic study shows that adsorbed oxygen on Cu−ZSM-5 desorbs during the pulse NO reaction. These results demonstrate the presence of two pathways for O_2 formation: oxygen produced from the decomposition of $Cu^{2+}(NO_3^-)$ and oxygen from the desorption of adsorbed oxygen on Cu−ZSM-5.

Introduction

Various analytical techniques have been used to study the active sites and reaction intermediates for the direct nitric oxide (NO) decomposition reaction over Cu−ZSM-5.[1−16] Electron paramagnetic resonance spectroscopy (EPR),[3,8] X-ray photoelectron spectroscopy (XPS),[13,17] Cu^+ luminescence spectroscopy,[10] and infrared (IR) spectroscopy of NO and CO adsorption[2−9,11−13] have identified the Cu^+ and Cu^{2+} states in Cu−ZSM-5. It has been shown that exposure of the Cu^+ ions to NO oxidizes them to Cu^{2+} with the formation of adsorbed oxygen.[2,3,6,8] Desorption of oxygen could result in the reduction of Cu^{2+} species to the Cu^+ species.[8]

The majority of the NO adsorption studies over Cu−ZSM-5 were conducted at 0.07−39.9 Torr of NO and 77−303 K. IR studies of NO adsorption have identified various forms of NO adsorbate species: $Cu^+(NO)$ (1814 cm^{-1}), $Cu^+(NO)_2$ (1733 and 1835 cm^{-1}), $Cu^{2+}(O^-)(NO)$ (1895 cm^{-1}), $Cu^{2+}(NO)$ (1910 cm^{-1}), NO^+ on cationic positions in the zeolite or NO_2^+ on Brønsted acid (BA) sites (2124 cm^{-1}), and NO_x ($x = 2$ or 3) species (1624, 1601, 1575, 1315 cm^{-1}).[2−9,11−13,20] In situ studies at temperatures above 573 K show the NO_x species exhibiting dominant IR bands while the $Cu^+(NO)$, $Cu^{2+}O^-(NO)$, and $Cu^{2+}(NO)$ species appear with attenuated IR bands.

The lack of separate spectroscopic techniques for the verification of IR band assignments has led to uncertainty in the nitrato-group ($M-NO_3$ where M is a metal ion), nitrito group (M−O−N═O), and nitro-group ($M-NO_2$) assignment during NO adsorption over Cu−ZSM-5. The band at 1628 cm^{-1} has been recently attributed to the nitro group associated with the Cu^{2+} ion, and the bands at 1572 and 1594 cm^{-1} have been attributed to the nitrate ions.[18] In contrast, the classical assignment of the nitrato group, nitrito group, and nitro group was based on the IR spectra of NO_x ($x = 1$ or 2) complexes which showed that a majority of the bridged nitrato complexes were observed at wavenumbers greater than 1600 cm^{-1}; the chelating nitrato species were observed at wavenumbers below 1600 cm^{-1}; the nitrito and nitro complexes were observed at wavenumbers below 1500 cm^{-1}.[19] Recent studies have also suggested that the band at 2133 cm^{-1}, which was previously assigned to NO_2^+ species adsorbed on the BA site,[9] can be assigned to the NO^+ species occupying the cationic positions in the zeolite.[20] Earlier isotopic studies have suggested that this band can be assigned to either NO^+ or NO_2^+ species on the BA site.[21] The present study follows the classical assignment: the bands at wavenumbers greater than 1600 cm^{-1} (1623 and 1610 cm^{-1}) were attributed to bridged nitrato species adsorbed on the Cu^{2+} ion, the band at 1575 cm^{-1} was attributed to the chelating nitrato species adsorbed on the Cu^{2+} ion, and the band at 2133 cm^{-1} was attributed to the adsorbed NO^+ species on cationic positions in the zeolite ($NO^+_{ad.}$).

Although the structures of a majority of NO adsorbates have been determined, little study has correlated adsorbate intensities with catalyst activity and selectivity. Separate IR and reaction studies do not provide a coherent picture of reactive adsorbates important to the reaction because the catalysts tested may not be exposed to an identical reaction environment.

The objective of the present study is to investigate for the first time the dynamic behavior of adsorbates, reactants, and products during NO decomposition on the under- and overexchanged Cu−ZSM-5. IR spectra of adsorbates as well as reactant and product profiles were obtained during temperature-programmed reaction (TPR), temperature-programmed desorption (TPD), and step/pulse switch transient experiments. Dynamic behavior of adsorbates, reactants, and product profiles

* To whom correspondence should be addressed.

10.1021/jp984112c CCC: $18.00
Published on Web 06/24/1999

were used to verify the proposed reaction intermediates and steps for N_2, N_2O, and O_2 formation.

Experimental Section

The underexchanged Cu−ZSM-5 was prepared by Johnson Matthey and supplied by the catalyst bank of Sandia National Laboratories. The extent of copper exchange was determined to be 83% (amount of exchange = 2(moles of Cu/moles of Al)),[15] the Si/Al ratio to be 24, and the amount of Na to be 34 ppm by inductively coupled plasma (ICP) emission spectroscopy (Galbraith Labs. Inc., Knoxville, TN). The underexchanged catalyst was characterized by X-ray diffraction (XRD), and its XRD pattern closely resembled that of ZSM-5.[22]

The overexchanged Cu−ZSM-5 sample was prepared by performing repeated copper exchange on 5 g of underexchanged catalyst using a 0.07 M solution of copper acetate. Cu−ZSM-5-83 (83 indicating the % Cu exchange), i.e., the underexchanged Cu−ZSM-5, was added to the copper acetate solution and continuously stirred for 24 h. The pH of the solution was maintained at 6.7 during the exchange. The solution was filtered, washed with distilled water, and dried in air at 373 K. The ion-exchange process was repeated on the dry sample obtained. The sample obtained from the repeated ion-exchange process was analyzed by ICP emission spectroscopy, and the amount of exchange was determined to be 127% (Cu/Al = 0.635) with a Si/Al ratio of 24. The overexchanged sample was labeled as Cu−ZSM-5-127.

For IR studies, 25 mg of catalyst powder was pressed into a self-supporting disk and placed in the IR beam path in the reactor cell.[23] Two more disks, pressed and broken down into flakes, were placed near the self-supporting disk and were subject to the same conditions as the disk in the IR reactor cell. The additional catalyst was added to increase the conversion of nitric oxide and to obtain a strong signal for the reactor effluent analysis by the mass spectrometer (MS). The Cu−ZSM-5 samples were pretreated in flowing He (autoreduction) at 773 K for 2 h and cooled to the desired temperature prior to each experiment unless specified otherwise. TPR studies were conducted by exposing the catalysts to a steady-state 5% NO in He stream followed by heating the reactor from 303 to 773 K at a heating rate of 10 K/min. For TPD studies, the catalysts were exposed to $^{15}N^{18}O$ flow for 10 min at 303 K, flushed with He, and heated from 303 to 798 K at a heating rate of 10 K/min in flowing He.

Step and pulse transient techniques were used in the present study to examine the dynamic behavior of adsorbates and the sites onto which they adsorb. The step technique, illustrated in Figure 1a, involved the switching of flow from He (5 cm^3/min) to NO/Ar (1/1) (5 cm^3/min) while maintaining the flow rate of the carrier gas (He) constant. The pulse reaction technique illustrated in Figure 1b involved the introduction of (a) 1 cm^3 of NO into the He stream over Cu−ZSM-5-83 and Cu−ZSM-5-127 at 308 K and (b) 0.5 cm^3 of NO into the He (40 cm^3/min) stream over Cu−ZSM-5-127. The 0.5 cm^3 pulse switch was performed at two different conditions: (a) pulse 0.5 cm^3 of NO over autoreduced Cu−ZSM-5-127 at 673−773 K and (b) pulse 0.5 cm^3 of NO at 673−773 K over Cu−ZSM-5-127 which was previously exposed to isotopic $^{15}N^{18}O$ TPD studies.

A Fourier transform infrared spectrometer (FTIR) (Nicolet Magna-IR 550) and an MS determined the changes in the adsorbate and product concentrations, respectively. Two mass spectrometers were used in this study: a Prisma QMS 200 (Pfeiffer Vacuum Technology) and a QMG 112 A (Balzers-Pfeiffer). The sampling speed of the QMS 200 was decreased due to its ability to monitor a larger number of species when compared to the QMG 112 A model. The MS profiles of the reactant and product gaseous species were multiplied by the respective calibration factors to obtain the elution rate profiles. It should be pointed out here that the calibration factor for gaseous NO_2 could not be obtained due to the lack of reliable NO_2 calibration gas. Hence, instead of the MS rate profiles, NO_2 intensity profiles are presented in the present study. Increase in the rate profiles of the N_2, O_2, N_2O, and NO_2 indicates an increase in their formation rates. The NO effluent rate profile indicated the response of unconverted NO eluting from the reactor cell. Lower NO effluent rates indicates higher NO conversion.

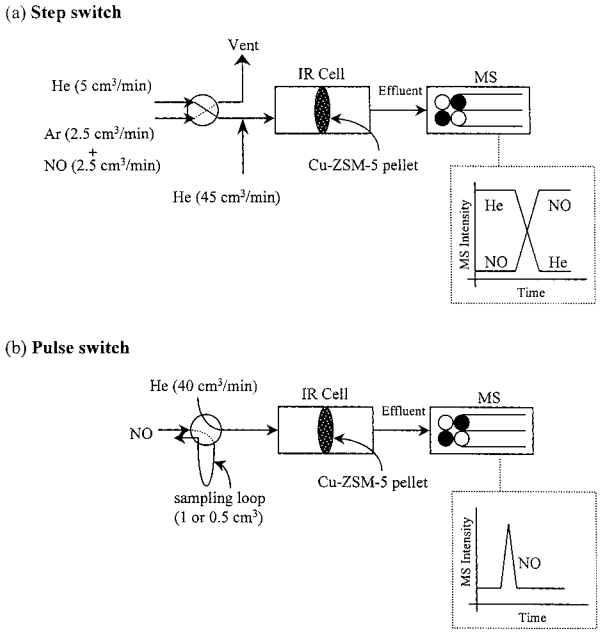

Figure 1. Illustration of the (a) step and (b) pulse transient technique.

Results

CO Adsorption Studies. The FTIR spectra of autoreduced Cu−ZSM-5-83 and Cu−ZSM-5-127 after exposure to 5% CO flow at 303 K for 0.5 and 10 min are shown in Figure 2. CO adsorption for 0.5 min over both the catalysts produced Cu^+-(CO) at 2157 cm^{-1} and adsorbed CO on water containing Cu^+ sites at 2139 cm^{-1}.[6,7,11,21] Increasing CO exposure for 10 min produced the symmetric vibration of $Cu^+(CO)_2$ at 2177 cm^{-1}, its asymmetric vibration at 2150 cm^{-1}, and adsorbed CO weakly bound to Lewis acid centers in the zeolite at 2112 cm^{-1}.[7] The $Cu^+(CO)$ species observed after 0.5 min exposure to 5% CO is equivalent to the $Cu^+(CO)$ species observed at low CO concentrations; $Cu^+(CO)_2$ observed at 10 min is equivalent to those found at high CO concentration.[6,7,11]

Temperature-Programmed Reaction (TPR). Figure 3 shows the IR spectra, MS profiles of the reactor effluent, and difference IR spectra during the 5% NO TPR over autoreduced Cu−ZSM-5-83. Exposure of the catalyst to 5% NO flow at 323 K resulted in the appearance of $Cu^{2+}O^-(NO)$ at 1890 cm^{-1}, bridged $Cu^{2+}(NO_3^-)$ at 1627 cm^{-1} (overlapped by the band at 1610 cm^{-1}), and chelating $Cu^{2+}(NO_3^-)$ at 1570 cm^{-1} as shown in Figure 3a. Increase in temperature led to changes in the IR intensity of adsorbate species (Figure 3a) and changes in the MS profiles of gaseous reactor effluents NO, N_2, O_2, N_2O, and NO_2 as shown in Figure 3b. Temperature increase from 523 to 673 K led to the decrease of bridged $Cu^{2+}(NO_3^-)$ intensity

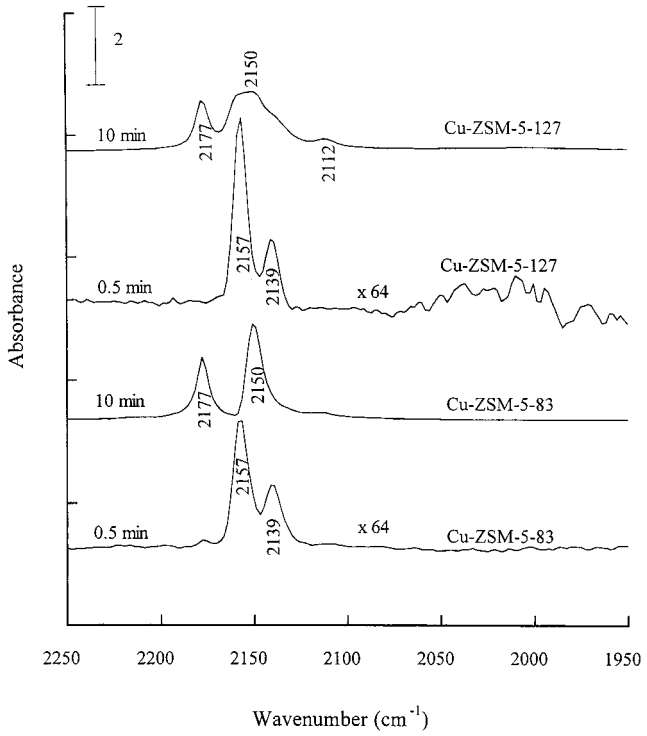

Figure 2. FTIR spectra of autoreduced Cu−ZSM-5-127, Cu−ZSM-5-83 at 0.5 min and autoreduced Cu−ZSM-5-127, autoreduced Cu−ZSM-5-83 at 10 min during exposure to 5% CO flow at 303 K.

concurrent with an increase in $Cu^{+}(NO)$ intensity to 623 K and increase in NO conversion and N_2O formation. Formation of O_2 appeared to commence at 653 K; however, continuous increase in the NO_2 profile from 523 K suggested that O_2 formation actually commenced at 523 K as O_2 may react with the effluent NO in the reactor downstream forming NO_2.[24] The differential spectra shown in Figure 3c for 773−523 and 773−423 K show that the intensity of bridged $Cu^{2+}(NO_3^{-})$ decreased in the 523−773 K region where N_2O, NO_2, and O_2 were produced.

Exposure of Cu−ZSM-5-127 to 5% NO at 323 K during TPR produced $Cu^{2+}(NO_3^{-})$ (bridged and chelating) similar to that observed over Cu−ZSM-5-83 with additional adsorbates including $Cu^{2+}(NO)$ at 1909 cm^{-1}, $NO^{+}_{ad.}$ at 2130 cm^{-1}, and a weak $Cu^{+}(NO)$ at 1814 cm^{-1} as shown in Figure 4a. Temperature increase from 323 to 773 K led to the decrease in intensities of bridged and chelating $Cu^{2+}(NO_3^{-})$, $Cu^{2+}(NO)$, and $NO^{+}_{ad.}$ corresponding to an increase in NO conversion and formation of N_2, O_2, N_2O, and NO_2 as observed in Figures 4a and 4b, respectively. The sudden increase of NO (m/e = 30) MS intensity in the 723−773 K region is attributed to the contribution from a fragment of NO_2 (m/e = 46) species to the intensity of the m/e = 30 species.[25] Difference spectrum for 723−423 K in Figure 4c shows that the bridged $Cu^{2+}(NO_3^{-})$ at 1624 cm^{-1} and $Cu^{2+}O^{-}(NO)$ at 1885 cm^{-1} decreased their intensities with temperature. The difference spectrum for 773−573 K also shows that the bridged $Cu^{2+}(NO_3^{-})$ and $Cu^{+}(NO)$ at 1813 cm^{-1} decreased their intensities with temperature. These species, however, remained on the surface at 723 K where N_2, O_2, N_2O, and NO_2 were produced. This observation raised the question of whether these species are involved in the decomposition reaction mechanism.

The major differences between Cu−ZSM-5-83 and Cu−ZSM-5-127 TPR were that (a) Cu−ZSM-5-127 was significantly more active than Cu−ZSM-5-83 and (b) $Cu^{+}(NO)$ emerged at 423 K over Cu−ZSM-5-127 and at 523 K over Cu−ZSM-5-83, indicating that the overexchanged copper was more facile to be autoreduced than underexchanged copper.

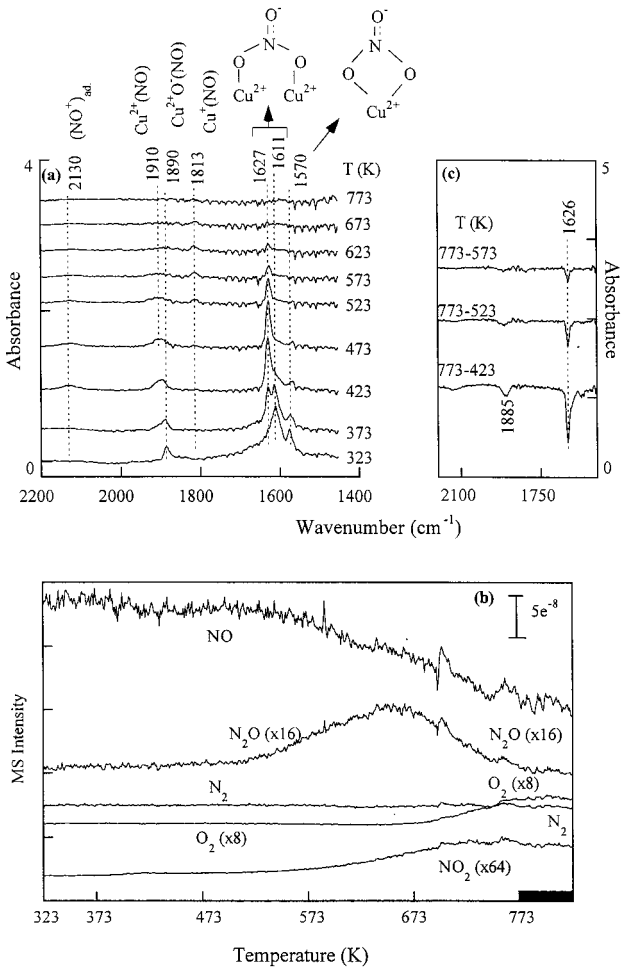

Figure 3. (a) IR spectra, (b) MS reaction profiles of the gaseous species during the temperature-programmed reaction (TPR) over underexchanged Cu−ZSM-5-83 (W/F = 2.2 g·s cm^{-3}) in a 5% NO in He stream, and (c) differential IR spectra obtained by subtracting the spectra at a particular temperature from a spectra at another temperature.

NO Step Switch at 308 K. FTIR spectra and MS profiles during a NO step switch provide (a) the sequence of formation of adsorbates and reactor effluents, (b) observation of interconversion of adsorbates, and (c) correlation of adsorbate intensity with concentration profiles of the reactor effluents in the transient and steady-state conditions during NO flow. Figure 5 shows a series of FTIR spectra of Cu−ZSM-5-127 during a step switch from He to 5% NO at 308 K. Initial exposure to the NO stream for 0.6 min produced $Cu^{2+}(NO)$, $Cu^{2+}O^{-}(NO)$, $Cu^{+}(NO)_2$, $Cu^{+}(NO)$, $NO^{+}_{ad.}$, and adsorbed N_2. The changes in the adsorbate intensity were accompanied by elution of unconverted gaseous NO and formation of N_2 as shown by the MS profiles in Figure 6a−c.

N_2 was the only product observed from the MS profiles and lasted for 0.3 min. Formation of N_2 from NO without producing O_2 suggests the occurrence of the stoichiometric reaction 2NO + 2S → N_2 + 2O−S, where S indicates surface sites. The adsorbed oxygen, O−S, interacts with other NO adsorbates and results in a decrease in the intensities of $Cu^{+}(NO)$ and $Cu^{+}(NO)_2$ as well as an increase in the intensities of $Cu^{2+}(NO_3^{-})$ (bridged and chelating) during the first 5 min of NO exposure. Continuous NO exposure did not produce any gaseous products, but the $Cu^{2+}(NO_3^{-})$ species (bridged and chelating) show

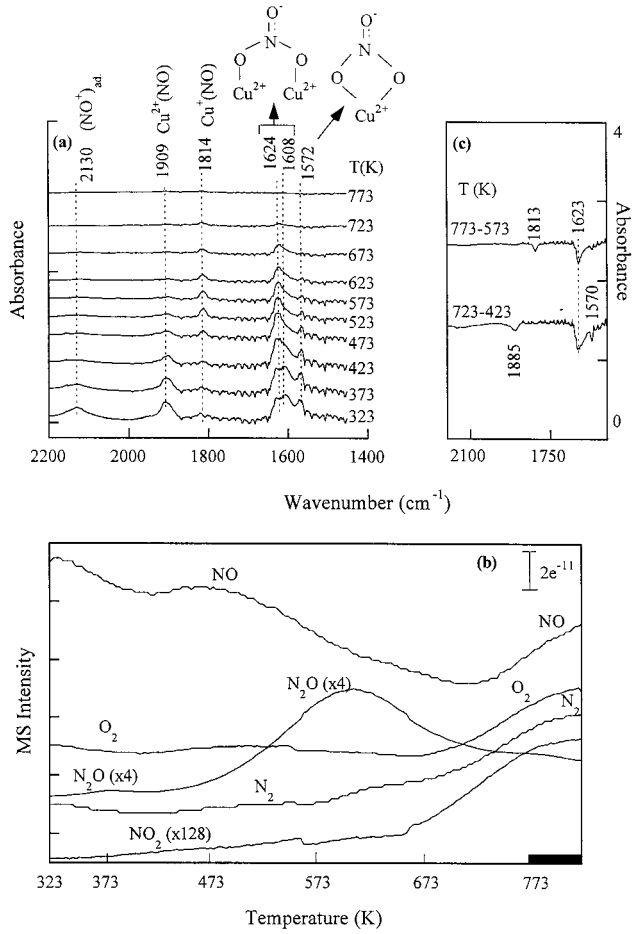

Figure 4. (a) IR spectra, (b) MS rate profiles of the gaseous species during the temperature-programmed reaction (TPR) over overexchanged Cu−ZSM-5-127 ($W/F = 2.2$ g•s cm^{-3}) in a 5% NO in He stream, and (c) differential IR spectra obtained by subtracting the spectra at a particular temperature from a spectra at another temperature.

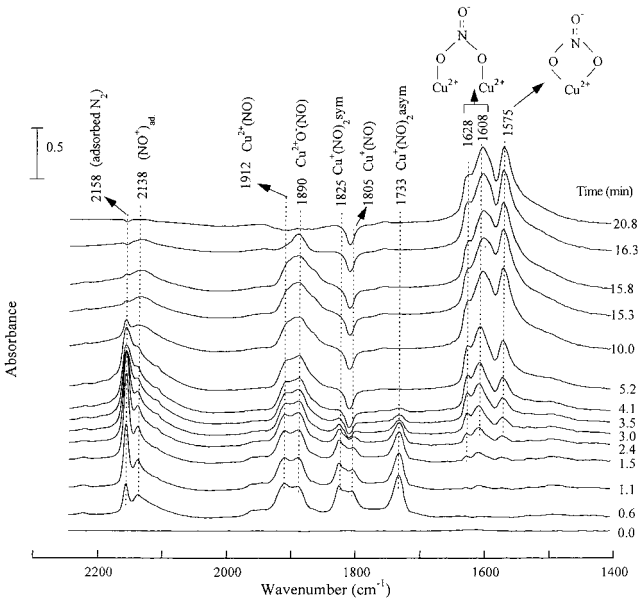

Figure 5. FTIR spectra of autoreduced Cu−ZSM-5-127 at 308 K during the 5% NO step switch ($W/F = 2.2$ g•s cm^{-3}).

continuous increase to 10 min. Then, all the adsorbate intensities leveled off and remained constant. Switching off NO, at 20.7 min, caused a decrease in the intensity of adsorbed N_2, $NO^+_{ad.}$, $Cu^{2+}(NO)$, and $Cu^{2+}O^-(NO)$, but the intensity of $Cu^{2+}(NO_3^-)$ (bridged and chelating) species did not change.

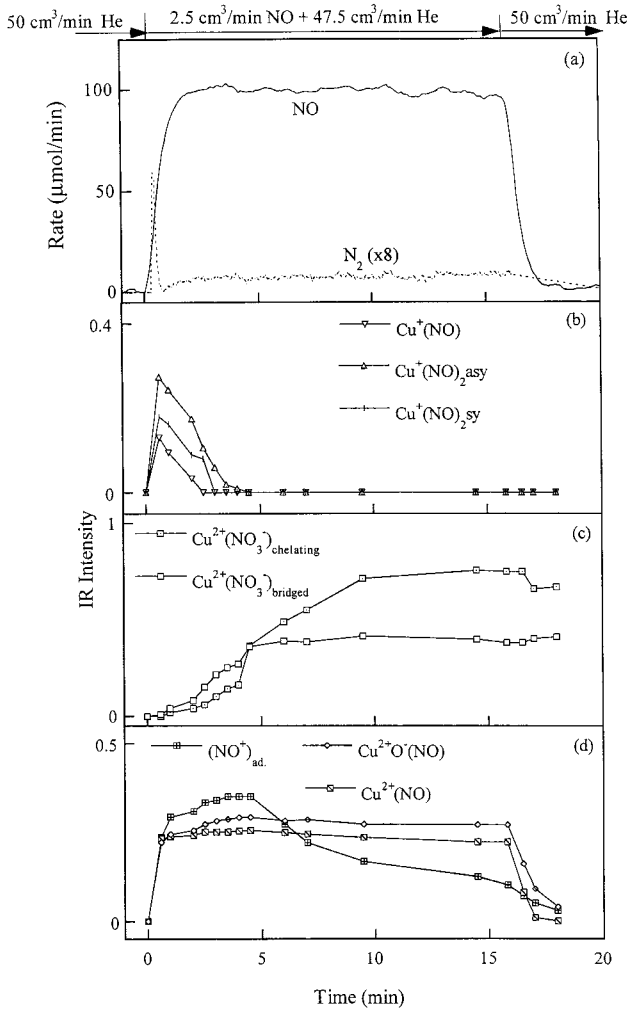

Figure 6. (a) MS rate profiles of reactor effluents NO and N_2; (b), (c), and (d) integrated FTIR intensity vs time for $Cu^+(NO)$, $Cu^+(NO)_2$, $Cu^{2+}(NO_3^-)$, $NO^+_{ad.}$, $Cu^{2+}(NO)$, and $Cu^{2+}O^-(NO)$ adsorbate species during 5% NO ($W/F = 2.2$ g•s cm^{-3}) step switch at 308 K.

NO Pulse at 308 K. The pulse switch, similar to the step switch described earlier, examines and correlates the sequence of adsorbates and reactor effluents during the NO decomposition reaction. An interesting difference is that while the step switch allows observation of interconversion of adsorbates in the steady-state NO flow, the pulse switch provides the same information in the steady-state inert He flow. Figure 7 shows the MS intensity profiles and rapid scan IR spectra during 1 cm^3 of NO pulse switches in He flow over Cu−ZSM-5-127 at 308 K. Introduction of the first 1 cm^3 of NO pulse over autoreduced Cu−ZSM-5-127 resulted in the conversion of NO to N_2 as shown by the increase of the N_2 MS profile in Figure 7a. Exposure to the NO pulse at 308 K also led to the formation of adsorbed N_2O at 2220 cm^{-1} and $Cu^{2+}(NO)$, $Cu^{2+}O^-(NO)$, $Cu^+(NO)_2$ and $Cu^+(NO)$ as shown in Figure 7b. The $Cu^{2+}(NO)$, $Cu^+(NO)_2$, and $Cu^+(NO)$ adsorbate species decreased in intensity faster than adsorbed N_2O, which disappeared faster than the $Cu^{2+}O^-(NO)$ species.

An additional 1 cm^3 of NO pulse switches did not decompose NO to produce N_2 as shown in the MS profiles for the third NO pulse in Figure 7a. However, additional exposure to NO led to the formation of chelating and bridged $Cu^{2+}(NO_3^-)$ species evidenced by the observation of bands at 1575 and 1607

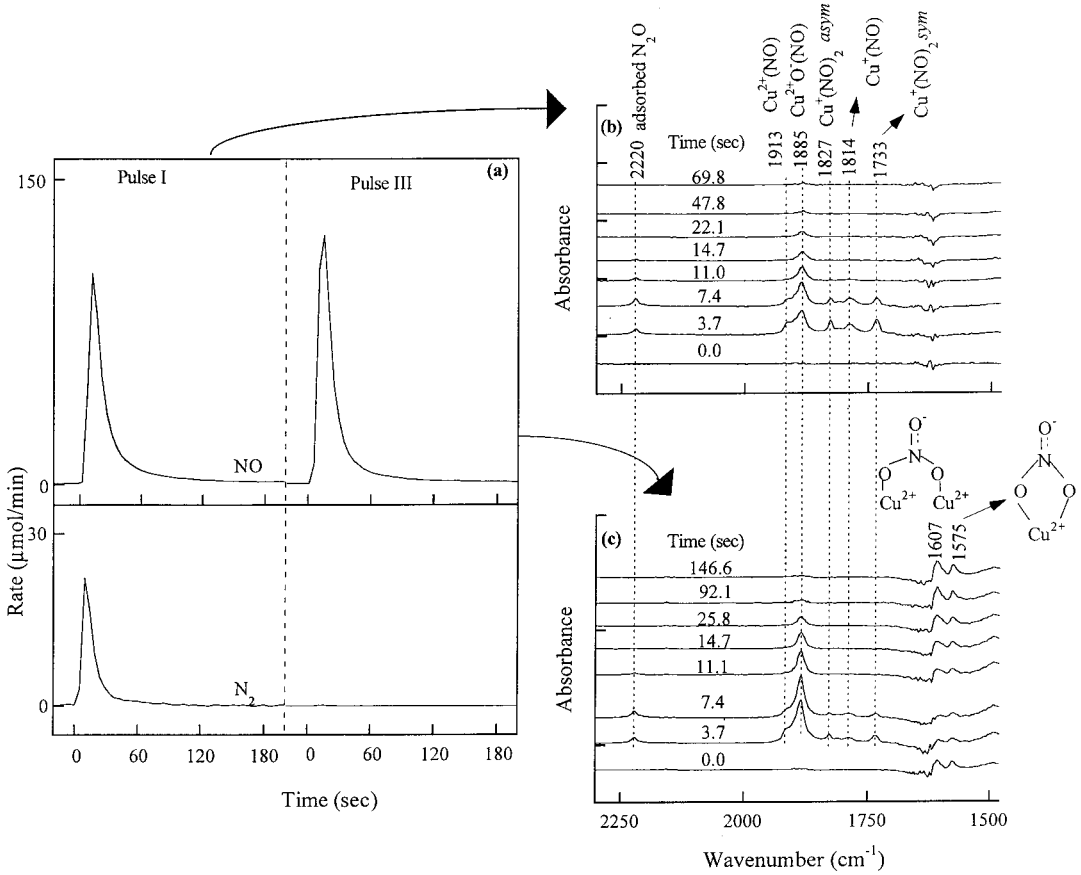

Figure 7. (a) MS rate profiles of the reactor effluent during 1 cm^3 of NO pulses at 308 K over autoreduced Cu−ZSM-5-127, (b) FTIR rapid scan spectra during the first NO pulse, and (c) third NO pulse.

cm^{-1} at 0.0 min. These species are shown in Figure 7c prior to the introduction of the third NO pulse switch. The variation of adsorbate intensities with the MS effluent rate profile of NO during the third NO pulse is shown in Figure 8. Exposure of the catalyst sample to the third NO pulse caused a decrease in the intensity of chelating and bridged $Cu^{2+}(NO_3^-)$ species and an increase in the intensity of $Cu^{2+}O^-(NO)$ during the presence of NO on the surface. Disappearance of NO at the end of the third pulse restored the chelating and bridged $Cu^{2+}(NO_3^-)$ species but to an intensity higher than that prior to the introduction of the third NO pulse. The intensity of $Cu^{2+}O^-(NO)$ observed during the third NO pulse was higher than that during the first pulse indicating an increase in Cu^{2+} sites due to the NO pulse.

NO Step Switch at 673 K. Figure 9 shows a series of FTIR spectra of autoreduced Cu−ZSM-5-83 and Cu−ZSM-5-127 during the step switch from He to 5% NO at 673 K. Initial NO exposure of Cu−ZSM-5-83, following the switch from He to the 5% NO stream (step up), led to the formation of $NO^+_{ad.}$ and $Cu^+(NO)$ as shown by the spectra at 12.5 min (Figure 9a). Further exposure to NO led to the appearance of $Cu^{2+}O^-(NO)$ and bridged $Cu^{2+}(NO_3^-)$. During the increasing exposure to NO, bridged $Cu^{2+}(NO_3^-)$ species increased in intensity slower than $NO^+_{ad.}$, $Cu^+(NO)$, and $Cu^{2+}O^-(NO)$ species. After 15.5 min of exposure to NO, the intensity of all the observed IR species reached a maximum. Switching the flow from 5% NO back to He (step down) led to the immediate disappearance of $Cu^{2+}O^-(NO)$ and $Cu^+(NO)$ as well as a gradual decrease in the $NO^+_{ad.}$ and bridged $Cu^{2+}(NO_3^-)$ intensities.

Figure 9b shows a series of FTIR spectra of autoreduced Cu−ZSM-5-127 during the step switch from He to 5% NO at 673 K. Cu−ZSM-5-127 produced the same type of adsorbates as Cu−ZSM-5-83, but with different intensities and time sequences. Cu−ZSM-5-127 allows immediate formation and disappearance of $Cu^+(NO)$ and bridged $Cu^{2+}(NO_3^-)$ during the step switch with NO on and off. These characteristics of adsorbates on Cu−ZSM-5-127 may be related to its high activity and selectivity for NO decomposition to N_2 and O_2. The step switch MS effluent rate profiles in Figure 10a,b show that Cu−ZSM-5-127 is significantly more active and selective for direct NO decomposition than Cu−ZSM-5-83. Table 1 shows the activity and selectivity of both catalysts at 673 K.

Temperature-Programmed Desorption of $^{15}N^{18}O$. Figure 11 illustrates a series of FTIR spectra and differential spectra of Cu−ZSM-5-127, and Figure 12 shows the MS profiles of reactor effluent during $^{15}N^{18}O$ TPD over autoreduced Cu−ZSM-5-127. Prior to flowing $^{15}N^{18}O$ for the TPD study, the catalyst was subject to the NO pulse reaction at 673 K. Exposure to $^{15}N^{18}O$ at 303 K for 15 min and subsequent purge with He for 30 min led to the observation of prominent bands at 1587 and 1563 cm^{-1}as well as weak bands at 1623 and 1513 cm^{-1} as shown in Figure 11a. MS profiles during the TPD in Figure 12 show that species associated with ^{16}O desorbed in greater quantities than the ^{18}O species with increase in temperature although the Cu−ZSM-5-127 catalyst was subject to $^{15}N^{18}O$ flow. Observation of the ^{16}O desorbing species and $^{15}N^{16}O$-containing adsorbed nitrates (described later) suggests that exchange occurred between ^{18}O species, from the $^{15}N^{18}O$ flow, and ^{16}O already present on the Cu−ZSM-5-127 surface during the $^{15}N^{18}O$ adsorption. The formation of product and adsorbate species associated with ^{16}O was further confirmed by calculating and comparing the predicted wavenumbers of the adsorbate species with the observed values as shown in Table 2. The calculation of wavenumbers of the isotopic species tabulated

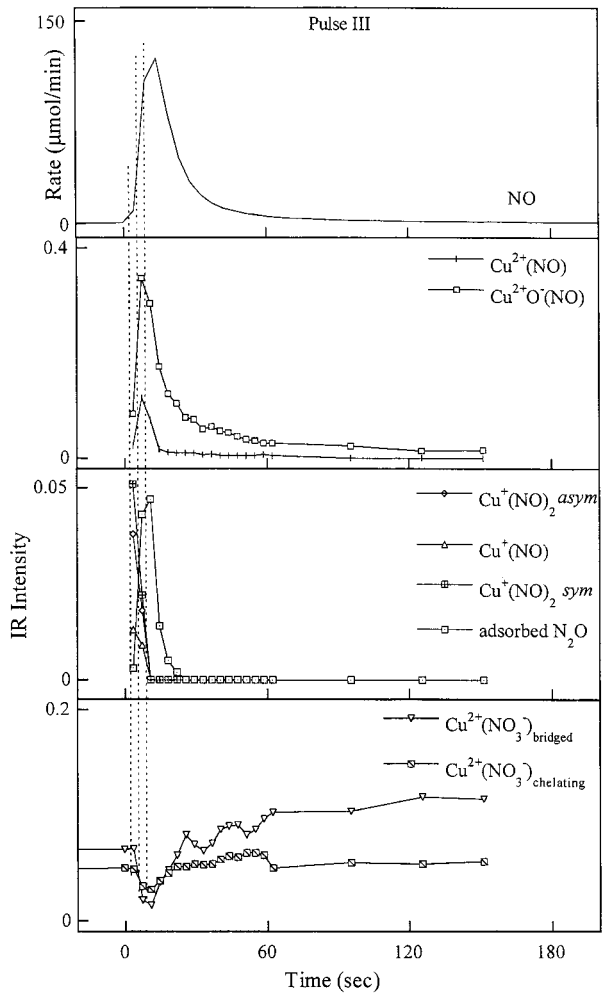

Figure 8. Variation of IR intensities of adsorbate species and MS rate profile of NO with time during the third 1 cm^3 of NO pulse over Cu−ZSM-5-127 at 308 K.

in Table 2 was based on the expression

$$\nu_{^{15}N^{18}O} = \nu_{^{14}N^{16}O}(\mu_{^{14}N^{16}O}/\mu_{^{15}N^{18}O})$$

where ν is wavenumber (cm^{-1}) and μ is reduced mass. This expression was based on the assumption that the potential energy changes of the constituent atoms in a bond can be approximated to that of a harmonic oscillator.[26]

Increase in temperature from 303 to 413 K led to a change in the intensity of bridged $Cu^{2+}(^{14}N^{16}O_3)^-$, chelating Cu^{2+}-$(^{15}N^{16}O^{?}O_2^-)$, and bridged $Cu^{2+}(^{15}N^{16}O^{?}O_2^-)$ corresponding to the desorption of gaseous (a) $^{15}N^{16}O$ in greater quantities than $^{15}N^{18}O$ and (b) $^{15}N_2{}^{16}O$ in greater quantities than $^{15}N_2{}^{18}O$ as shown in Figures 11a and 12. The calculation of wavenumbers for the isotopic $Cu^{2+}(NO_3^-)$ species was based on the assumption that the O atom in the $^{15}N-O$ bond is ^{16}O; however, the identity of the other two O atoms could not be established. Hence, the O atoms, whose identity is not established, are denoted by $^{?}O$.

$^{15}N_2{}^{16}O$ and $^{15}N_2{}^{18}O$ exhibit a desorption peak at 453 K. The desorption of $^{15}N_2{}^{16}O/^{15}N_2{}^{18}O$ ranges from 413 to 523 K where the IR spectra show a decrease in bridged $Cu^{2+}(^{15}N^{16}O^{?}O_2^-)$ intensity. Subsequent increase of temperature from 563 to 643 K led to the decrease in intensity of bridged $Cu^{2+}(^{14}N^{16}O_3^-)$, chelating $Cu^{2+}(^{15}N^{16}O^{?}O_2^-)$, and bridged $Cu^{2+}(^{15}N^{16}O^{?}O_2^-)$. The decrease in intensity was concurrent with the desorption of (a) $^{15}N^{16}O$ in greater quantities than $^{15}N^{18}O$, (b) $^{15}N_2{}^{18}O$ greater than $^{15}N_2{}^{16}O$, (c) $^{15}N^{16}O_2$ greater than $^{15}N^{16}O^{18}O$ and $^{15}N^{18}O_2$, and (d) $^{16}O_2$ greater than $^{18}O_2$. If the majority of $^{15}N^{16}O_2$ and $^{15}N^{16}O^{18}O$ desorbed from any form of the $Cu^{2+}(NO_3^-)$ species, part of the $^{?}O$ could be attributed to ^{16}O and part of it to ^{18}O. Production of more $^{15}N_2{}^{16}O$ than $^{15}N_2{}^{18}O$, more $^{16}O_2$ than $^{18}O_2$ from $^{15}N^{18}O$, suggests that ^{16}O associated with Cu−ZSM-5 is more accessible to the oxygen desorption pathway than ^{18}O during TPD. The desorption profiles obtained in the present study are comparable to the profiles obtained in a similar $^{15}N^{18}O$ TPD study.[27] The study suggested that the desorption of $^{16}O_2$ and $^{16}O^{18}O$ at temperatures greater than 523 K can be caused by the isotopic exchange between the ^{18}O species from the gaseous $^{18}O_2$ formed and the lattice oxygen (^{16}O) present on the catalyst surface.

NO Pulse Studies before and after $^{15}N^{18}O$ TPD. FTIR spectra of adsorbates as well as MS reactant and product profiles were acquired during 0.5 cm^3 of NO pulses over Cu−ZSM-5 before and after $^{15}N^{18}O$ TPD studies to determine the role of $Cu^{2+}(NO_3^-)$ in the formation of O_2 during NO decomposition. The MS rate profile of NO_2 could not be obtained; hence the MS intensity profile of the NO_2 species is provided in the inset. The MS rate profiles of the reactor effluent, variation of IR intensity of the $Cu^{2+}(NO_3^-)$ species, and rapid scan IR spectra of autoreduced Cu−ZSM-5-127 during the first 0.5 cm^3 of NO pulse at 673 K illustrated in Figure 13 show that (a) NO decomposition to gaseous N_2, O_2, and NO_2 was accompanied by the formation of $NO^+_{ad.}$, $Cu^+(NO)$, and bridged $Cu^{2+}(NO_3^-)$ species and (b) the intensity of bridged $Cu^{2+}(NO_3^-)$ reached a maximum and decreased to zero slower than the intensity of $NO^+_{ad.}$ and $Cu^+(NO)$ species. The MS rate profiles of reactor effluent, variation of IR intensity of the bridged $Cu^{2+}(NO_3^-)$ species, and rapid scan IR spectra of Cu−ZSM-5-127 previously exposed to $^{15}N^{18}O$ TPD presented in Figure 14 show that (a) NO decomposition produces $^{18}O^{16}O$ along with N_2, O_2, and NO_2 as well as prominent bands at 2120, 1814 and 1623 cm^{-1} and (b) the maximum intensity of $Cu^{2+}(NO_3^-)$ over $^{15}N^{18}O$-exposed catalyst was lower in intensity than that observed during the NO pulse over autoreduced Cu−ZSM-5 (Figure 13b). Continuous NO pulses did not cause any change in the intensity of bridged $Cu^{2+}(NO_3^-)$ species but did cause slight decreases in the gaseous $^{16}O^{18}O$ formation.

Discussion

Activity and Adsorbates. It has been well established that overexchanged Cu−ZSM-5 is significantly more active than the underexchanged catalyst. The differences in their activities have been attributed to the stability of Cu^+ and Cu^{2+} sites and facile regeneration of Cu^+ sites on the overexchanged catalyst.[12] The characteristic of Cu^+ regeneration[4,7,8,12,17] also distinguishes Cu−ZSM-5 from other zeolite and oxide-supported Cu catalysts.

The present study shows that overexchanged Cu−ZSM-5 (a) contained more Cu^+ sites in CO atmosphere at 303 K (Figure 2), (b) produced lesser $NO^+_{ad.}$ during NO decomposition at 673 K (Figure 9), (c) caused faster decay of the $Cu^{2+}(NO_3^-)$ species during the switch from NO to He (Figure 9), when compared to the underexchanged Cu−ZSM-5 catalyst, and (d) produced $Cu^+(NO)$ and $Cu^+(NO)_2$ at lower temperatures similar to the underexchanged Cu−ZSM-5 during NO decomposition (Figures 3 and 4). Observations (a) and (d) are consistent with the results reported in the literature and further support the importance of reducibility of Cu sites for NO decomposition.[7,21]

Sequence of Adsorbate Formation and Disappearance. Both the step and pulse switch results in Figures 5−7 show that the formation of NO adsorbates follow the order $Cu^+(NO)$,

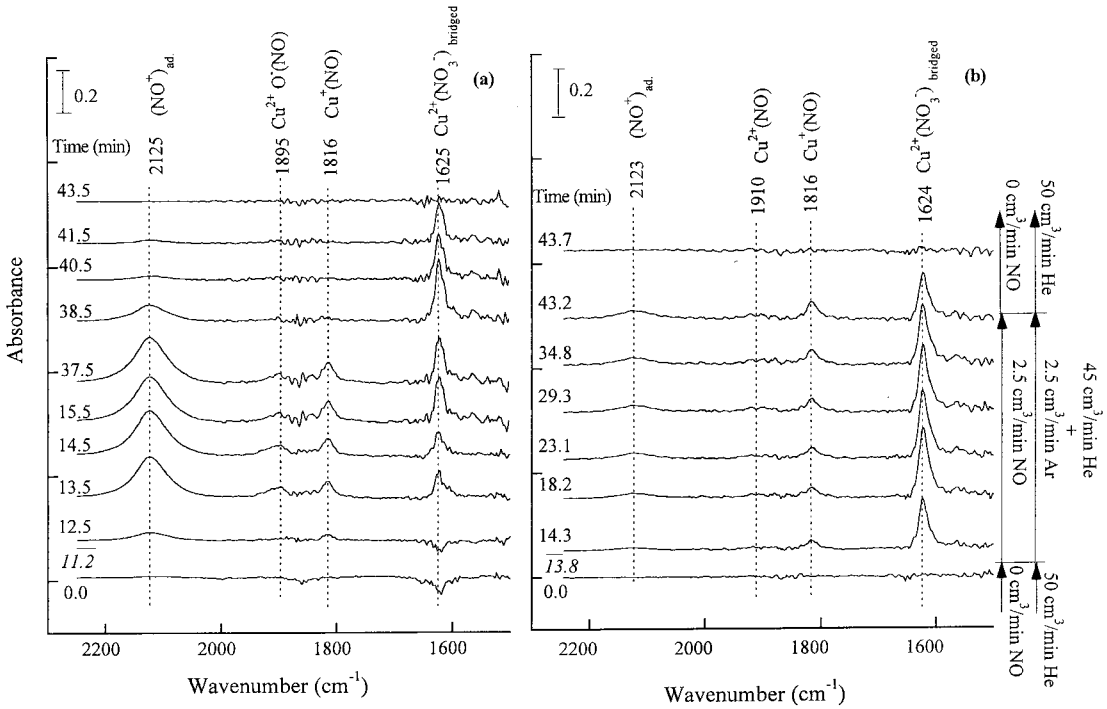

Figure 9. FTIR spectra of autoreduced (a) Cu−ZSM-5-83 and (b) Cu−ZSM-5-127 during the 5% NO (W/F = 2.2 g·s cm^{-3}) step switch at 673 K (the time in italics indicates the point of step switch from He to NO).

TABLE 1: Percent Conversion and Percent Yields during the 5% NO Step Switch over Cu−ZSM-5-83 and Cu−ZSM-5-127 at 673 K

	Cu−ZSM-5-83	Cu−ZSM-5-127
% conversion		
NO	14.7	21.1
% yields[a]		
N_2	0	40.5
O_2	0.2	03.7
N_2O	16.5	0
NO_2[b]	67.2	18.5

[a] % yield of A = (moles of A produced)/(moles of NO reacted). [b] % yield of NO_2 was calculated from the N balance of the reactor effluent (NO, N_2, O_2, and N_2O).

$Cu^+(NO)_2$, $Cu^{2+}(NO)$, $Cu^{2+}O^-(NO)$ > $NO^+_{ad.}$ > $Cu^{2+}(NO_3^-)$ at 308 K. The proposed steps[7] for the formation of these species are as listed below:

$$Cu^+ + NO \leftrightarrow Cu^+(NO) \quad (1)$$

$$Cu^+ + NO \leftrightarrow Cu^+(NO)_2 \quad (2)$$

$$Cu^{2+} + NO \leftrightarrow Cu^{2+}(NO) \quad (3)$$

$$Cu^{2+}O^- + NO \leftrightarrow Cu^{2+}O^-(NO) \quad (4)$$

$$S{-}O + NO \leftrightarrow S{-}O{-}NO^+ \quad (5)$$

S is a site on ZSM-5. The $NO^+_{ad.}$ species is represented as $S{-}O{-}NO^+$ in (5). Formation of the adsorbed species is reversible if the sites for their adsorption are available. The adsorbed species disappeared rapidly when either gaseous NO was removed or the Cu^+/Cu^{2+} site was oxidized/reduced. N_2 formation shot up during the growth/decay of $Cu^+(NO)$ and $Cu^+(NO)_2$ as well as during the growth of $Cu^{2+}(NO)$ and $Cu^{2+}O^-(NO)$ (Figure 6). Surprisingly, no direct correlation was observed between N_2 formation and variation in adsorbate intensity, especially with that of $Cu^+(NO)_2$. The lack of direct

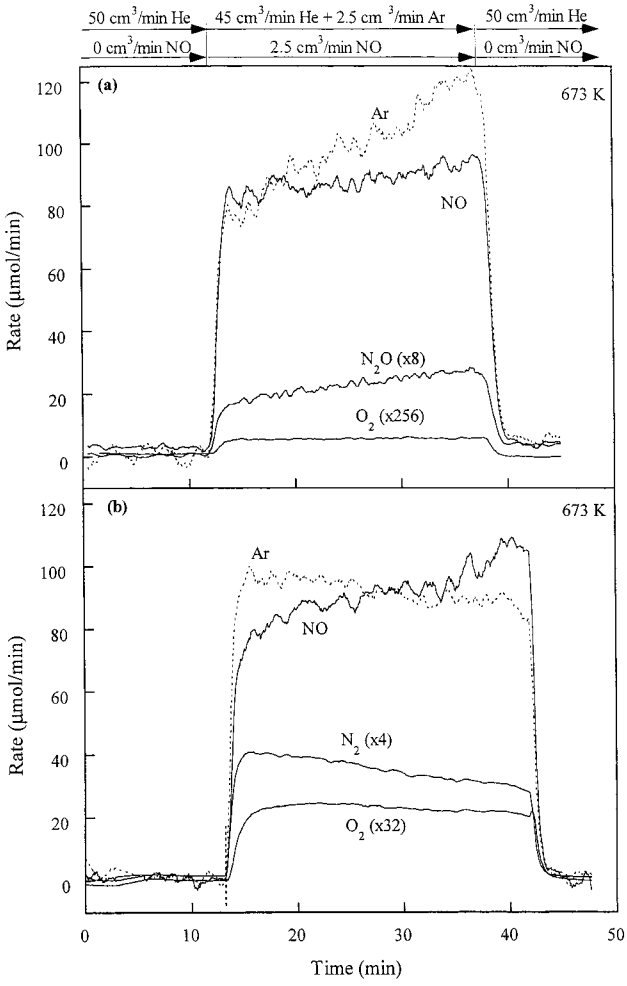

Figure 10. MS rate profiles of the reactor effluent during the 5% NO (W/F = 2.2 g·s cm^{-3}) step switch at 673 K over (a) Cu−ZSM-5-83 and (b) Cu−ZSM-5-127.

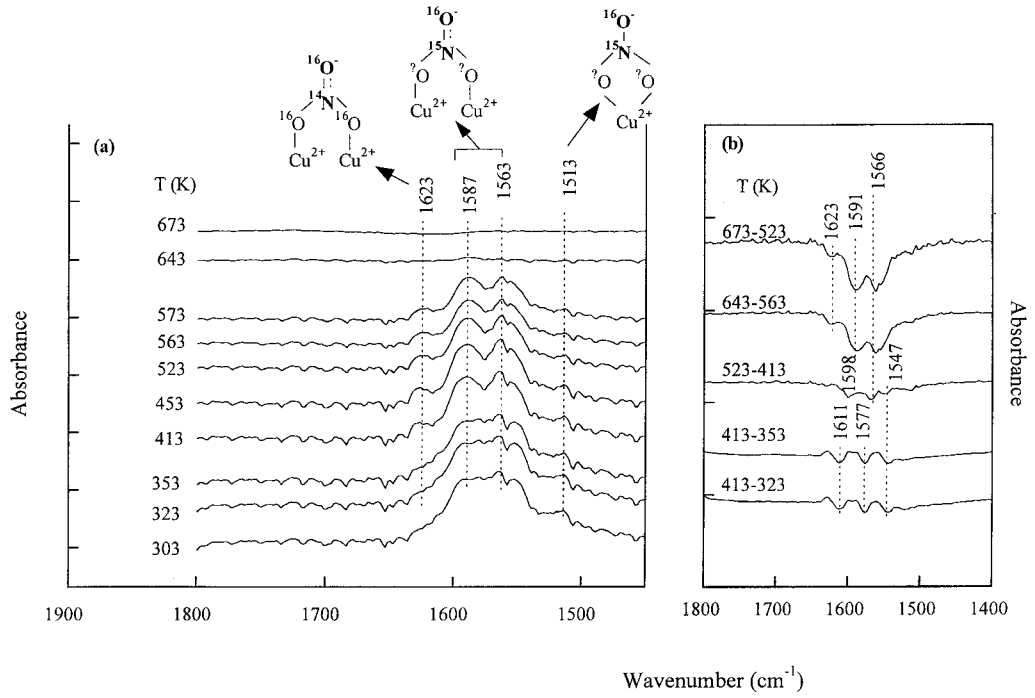

Figure 11. (a) FTIR spectra during temperature-programmed desorption of $^{15}N^{18}O$ over autoreduced Cu−ZSM-5-127 after exposure to 0.5 cm^3 of NO pulses at 673 K and (b) differential spectra at different temperatures during the TPD of $^{15}N^{18}O$ over Cu−ZSM-5-127.

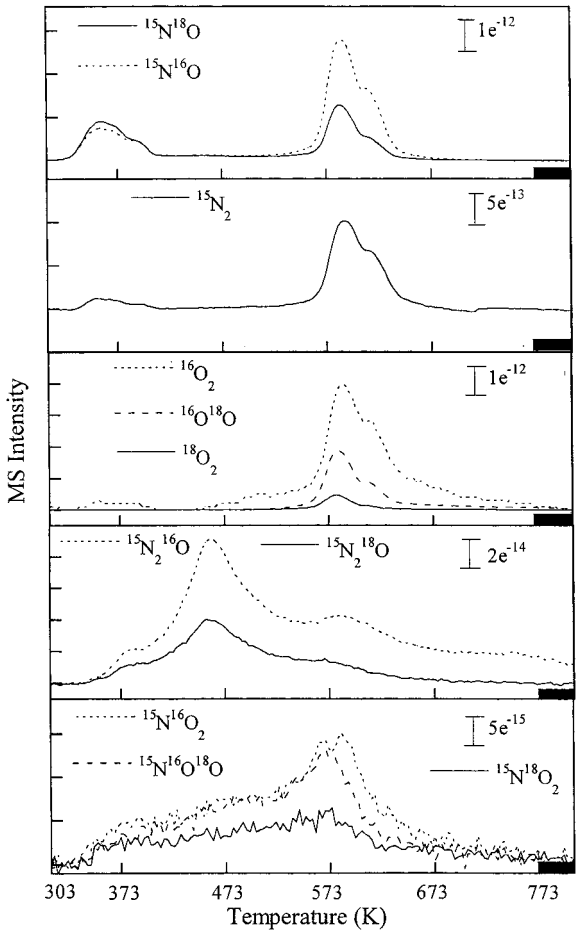

Figure 12. MS rate profiles of reactor effluent during $^{15}N^{18}O$ TPD over autoreduced Cu−ZSM-5-127 previously exposed to 0.5 cm^3 of NO pulses at 673 K.

correlation is evident from the fact that decrease in $Cu^+(NO)$/$Cu^+(NO)_2$ is not accompanied by N_2 formation (Figures 5−8). This observation did not directly support the widely accepted

TABLE 2: Assignment of FTIR Bands during $^{15}N^{18}O$ Flow over Cu−ZSM-5-127 at 308 K

adsorbate species	IR bands obsd during $^{14}N^{16}O$ flow (cm^{-1})	IR bands calcd (cm^{-1}) $^{15}N^{18}O$	IR bands calcd (cm^{-1}) $^{15}N^{16}O$	IR bands obsd during $^{15}N^{18}O$ flow (cm^{-1})
$NO^+_{ad.}$	2130	1942	2054	2093
$Cu^{2+}(NO)$	1910	1742	1842	1829
$Cu^{2+}O^-(NO)$	1890	1724	1822	1792
$Cu^+(NO)_2$	1824	1663	1759	−
	1734	1581	1672	−
$Cu^+(NO)$	1814	1654	1749	−
bridged $Cu^{2+}(NO_3^-)$	1628	1485	1570	1580
bridged $Cu^{2+}(NO_3^-)$	1608	1467	1551	1553
chelatin $Cu^{2+}(NO_3^-)$	1572	1434	1516	1523

mechanistic steps, shown below, that the $Cu^+(NO)_2$ species was an intermediate in the formation of N_2O and N_2:[2−4,7,28]

$$Cu^+(NO)_2 \rightarrow Cu^{2+}O^- + N_2O \quad (6)$$

$$Cu^+ + N_2O \rightarrow Cu^{2+}O^- + N_2 \quad (7)$$

These steps were proposed from separate IR and step switch studies on different catalysts.[2,3,7] $Cu^+(NO)_2$ was also observed on the underexchanged catalyst which produced N_2O at 303 K during the NO step switch.[29] $Cu^+(NO)_2$, however, was not observed at high temperatures (673 K). It has been pointed out that the $Cu^+(NO)_2$ species is formed at low temperatures and high NO partial pressures.[5,7,21] Thermodynamic calculations also confirm that the formation of $Cu^+(NO)_2$ species is not favorable at high temperatures.[30] Although lack of correlation between the N_2 and $Cu^+(NO)_2$ profiles ruled out the possible participation of $Cu^+(NO)_2$ as a precursor for N_2 formation, it did not eliminate N_2O as an intermediate for the formation of N_2. Figure 4 shows that, at temperatures above 610 K, the N_2O profile decreased while that of N_2 increased with temperature, suggesting that N_2O may serve as an intermediate for N_2 formation.

A key feature of the step and pulse switch results, shown in Figures 6 and 8, was the decrease in $Cu^+(NO)$ and $Cu^+(NO)_2$

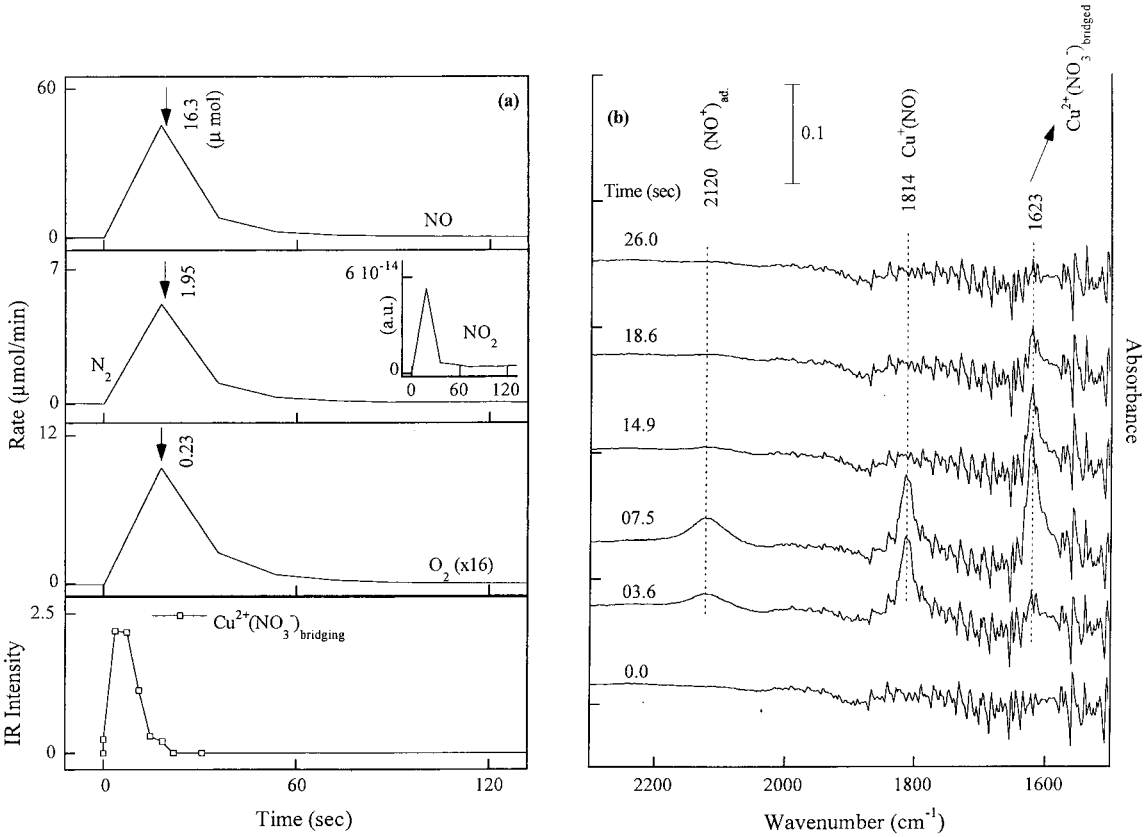

Figure 13. (a) MS rate profiles and IR intensity of the bridged $Cu^{2+}(NO_3^-)$ species and (b) FTIR rapid scan spectra during 0.5 cm^3 of NO pulse switch at 673 K over autoreduced Cu−ZSM-5-127.

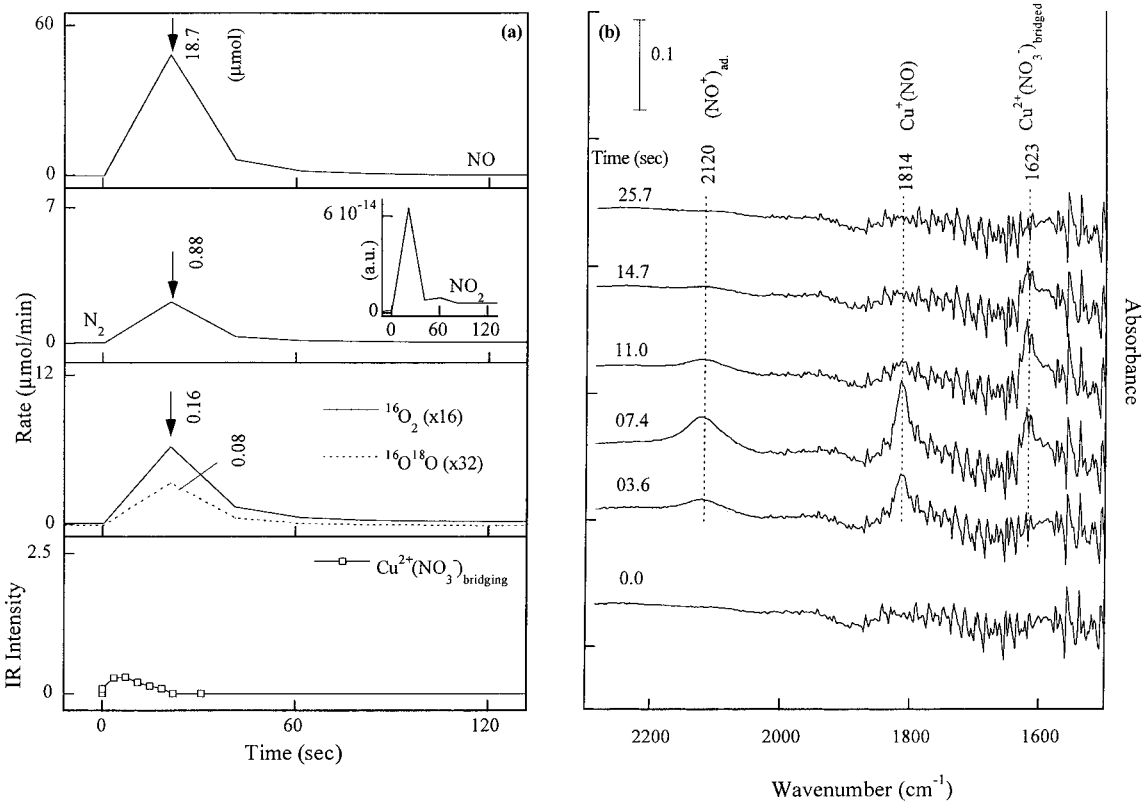

Figure 14. (a) MS rate profiles and IR intensity of the bridged $Cu^{2+}(NO_3^-)$ species and (b) FTIR rapid scan spectra during 0.5 cm^3 of NO pulse switch at 673 K over autoreduced Cu−ZSM-5-127 previously exposed to $^{15}N^{18}O$ TPD.

accompanied by increase in $Cu^{2+}(NO_3^-)$. The absence of $Cu^{2+}(NO_3^-)$ during N_2 formation in both step and pulse switch suggests that this species is not involved in the pathway for N_2 formation at 308 K. However, N_2 formation from adsorbed NO would leave adsorbed oxygen on the catalyst surface for reacting with other NO adsorbed species to form $Cu^{2+}(NO_3^-)$ as listed

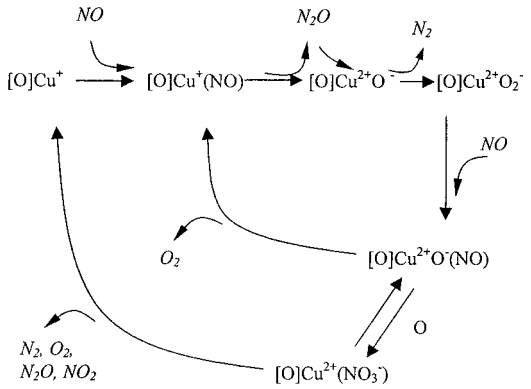

Reported pathways for N_2O and N_2 formation

Path I [2]

1. $Cu^{+} + NO \rightarrow Cu^{(1+\delta)}\text{-}NO^{\delta-}$
2. $2Cu^{(1+\delta)}\text{-}NO^{\delta-} \rightarrow Cu^{2+}\text{-}O\text{-}Cu^{2+} + N_2O\ (N_2)$

Path II [8]

1. $Cu^{2+} + NO \rightarrow Cu^{+}\text{-}(NO)^{+}$
2. $2Cu^{+}\text{-}(NO) \rightarrow (Cu\text{-}O\text{-}Cu)^{2+} + N_2O$

Path III [30]

1. $ZCu + NO \rightarrow ZCu\text{-}NO$
2. $ZCu\text{-}NO + NO \rightarrow ZCuO + N_2O$
3. $ZCuO + N_2O \rightarrow ZCuO_2 + N_2$

Figure 15. Proposed reaction scheme for NO decomposition over Cu−ZSM-5.

in the following equations.

$$Cu^{2+}O^{-} + O \rightleftharpoons Cu^{2+}O_2^{-} \quad (8)$$

$$Cu^{2+}O_2^{-} + NO \rightleftharpoons Cu^{2+}(NO_3^{-}) \quad (9)$$

The formation of $Cu^{2+}(NO_3^{-})$ indicated in (9), proposed by Bell and co-workers, has been demonstrated to be thermodynamically favorable at 773 K.[30] The negative charge associated with the NO_3 species of the bridged $Cu^{2+}(NO_3^{-})$ has been estimated from thermodynamical calculations to be − 0.245 and is consistent with the predicted geometry of the adsorbate.[30] The sequence of $Cu^{2+}(NO_3^{-})$ formation from $Cu^{+}(NO)$ may be simplified as follows:

$$Cu^{+}(NO),\ Cu^{+}(NO)_2 \xrightarrow[\text{step 1}]{\text{ads O}} Cu^{2+}(NO) \text{ or } Cu^{2+}O^{-}(NO) \underset{\text{step 2}}{\overset{\text{ads O}}{\rightleftharpoons}} Cu^{2+}(NO_3^{-})$$

The step 2 interconversion of $Cu^{2+}(NO_3^{-})$ and $Cu^{2+}O^{-}(NO)$ is supported by an increase in intensity of $Cu^{2+}O^{-}(NO)$ accompanied by a decrease in $Cu^{2+}(NO_3^{-})$ in Figure 8. $Cu^{2+}O^{-}(NO)$ appears to interact with the adsorbed O, obtained from NO dissociation, to form $Cu^{2+}(NO_3^{-})$. The migration of this adsorbed O can be inhibited by the silanation of the ZSM-5 surface.[32] An undisrupted/unmodified ZSM-5 surface is needed to facilitate the oxygen migration and formation of $Cu^{2+}(NO_3^{-})$ and O_2. Further isotopic studies are underway to understand this mechanism.

Among the adsorbed species, listed in steps 1 and 2, Cu^{+}-(NO) and $Cu^{+}(NO)_2$ are the most sensitive to the NO environment while $Cu^{2+}(NO_3^{-})$ is the least. Although $Cu^{+}(NO_3^{-})$ shows similar IR bands on the over- and underexchanged catalyst in Figures 3, 4, and 9, the species exhibits different thermal stability. Low stability of $Cu^{2+}(NO_3^{-})$ on the overexchanged catalyst reflects its high reactivity. These species appear to strongly adsorb on the underexchanged Cu−ZSM-5 but not on the overexchanged catalyst. The difference in stability must be resulting from the different chemical environment, which needs further investigation.

Figures 3 and 4 show the bridged $Cu^{2+}(NO_3^{-})$ species undergo decomposition to produce NO, N_2O, NO_2, and O_2. The rate of decomposition is faster on the overexchanged than the underexchanged catalyst. Comparison of the decay of $Cu^{2+}(NO_3^{-})$ on overexchanged and underexchanged Cu−ZSM-5 illustrated in Figure 9 shows that rate of decay on the overexchanged catalyst is faster than underexchanged Cu−ZSM-5. TPD studies (Figures 11 and 12) show that the $Cu^{2+}(NO_3^{-})$ species serves as a precursor for O exchange during $^{15}N^{18}O$ adsorption, and also decomposes to form N_2, O_2, N_2O, NO_2, and NO in the 323−723 K region. However, $Cu^{2+}(NO_3^{-})$ is not the main precursor responsible for O_2 formation since the amount of O_2 formation did not correlate with that of bridged $Cu^{2+}(NO_3^{-})$ as observed in Figures 13 and 14. Furthermore, Figure 14 shows that $^{18}O^{16}O$ was not produced from $Cu^{2+}(NO_3^{-})$. Absence of $N^{18}O^{16}O$ formation in Figure 14 rules out the reaction between NO and $^{18}O^{16}O$ and also suggests that NO_2 is formed from the bridged $Cu^{2+}(NO_3^{-})$.

The thermal stability and reactivity of the adsorbed NO species can be further examined by comparing adsorbates and products during temperature-programmed, step, and pulse switch reaction at 308 and 673 K. Observation of $Cu^{+}(NO)$, $Cu^{2+}(NO_3^{-})$, and $NO^{+}_{ad.}$ at 673 K suggests that the rate of adsorption of NO for the formation of $Cu^{+}(NO)$ is greater than the desorption rate and the reaction rate for the formation of $Cu^{2+}(NO_3^{-})$ is greater than the decomposition rate. The possible sequence of formation of these adsorbed species and gaseous products is illustrated in Figure 15, which does not include the detailed stoichiometry of each step. N_2 formation illustrated in Figure 15 is a low-energy process as evidenced by its formation at 308 K. The oxygen, indicated in Figure 15 as [O], is adsorbed on Cu−ZSM-5 in an unknown state that requires further investigation.

An important aspect of the NO decomposition mechanism is to explain the processes of N−O bond dissociation as well as N−N bond and O−O bond formation. The transient in situ IR technique, though very useful in obtaining information on the dynamic behavior of adsorbed species, cannot provide direct and unambiguous evidence for the elucidation of NO dissociation and O_2 formation. The present study attempts to explain N_2, N_2O, and O_2 formation in light of the literature and the present results of adsorbate behavior.

The formation of N_2O and N_2 from $Cu^{+}(NO)$ or $Cu^{+}(NO)_2$ is significantly more complicated than shown in Figure 15, since

no correlation between N_2O and N_2 formation and variation of $Cu^+(NO)/Cu^{2+}(NO)$ intensity was observed. Although the role of $Cu^+(NO)/Cu^+(NO)_2$ in N_2O and N_2 formation remains unclear, the need of Cu^+ for N_2 formation is evident by the observation of N_2 formation with the presence of $Cu^+(NO)$ in Figures 4, 6−9, 13, 14. The role of $Cu^+(NO)$ as a precursor for the formation of N_2O and N_2 has been reported earlier as shown in paths I, II, and III (Figure 15).[2,8,30] It should be pointed out here that paths I−III show the overall reaction pathway for N_2O and N_2 formation instead of the fundamental reaction steps. Path I proposed that $Cu^+(NO)$ reacts with a neighboring $Cu^+(NO)$ to release N_2O or N_2; path II showed that the desorption of NO led to the oxidation of Cu^+ to $(Cu-O-Cu)^{2+}$ at 373 K producing N_2O; path III suggested that ZCu−NO (Z is the anionic zeolite site to which Cu is bound) interacts with NO to release N_2O and form ZCuO, which upon reaction with N_2O produces N_2 and $ZCuO_2$. The first two steps of path III can be used to explain the formation of N_2O on the underexchanged catalyst.

The present study shows lack of correlation between $Cu^+(NO)$ and N_2 profiles which further supports the existence of an additional elementary step, possibly a rate-limiting step, between the depletion of $Cu^+(NO)$ and formation of N_2 as proposed by path III. The immediate overshoot in N_2 formation, shown in Figure 6, clearly demonstrates the facileness of N−N bond formation. Adsorbed N, from dissociated NO, is weakly bound on the copper and ZSM-5 surface, especially on the overexchanged Cu−ZSM-5. Thus we conclude that N_2O may not be the only precursor for N_2 formation. N_2 formation can occur by the combination of the readily available adsorbed N species.

NO_2 was found to be stable under NO decomposition conditions. Our temperature-programmed reaction of flowing NO_2 on Cu−ZSM-5-127 produced NO and N_2O instead of N_2 and O_2.[33] The absence of N_2 and O_2 formation suggests that NO_2 is not a precursor for N_2 formation.

$Cu^{2+}O^-$, instead of Cu^{2+}, is included in Figure 15 because the NO decomposition activity has been found to correlate with $Cu^{2+}O^-$.[31] The copper ions, Cu^+ and Cu^{2+}, appear to be associated with the lattice oxygen present in the zeolite support of the catalyst.[27] O_2 desorption from $Cu^{2+}O^-$ is essential for conversion of $Cu^{2+}O^-$ site to Cu^+. This step does not appear to be the rate-limiting step since Cu−ZSM-5 possesses significantly more $Cu^+(NO)$ than $Cu^{2+}O^-(NO)$, i.e., more Cu^+ than $Cu^{2+}O$ sites during NO decomposition at 673 K. In other words, the dominance of $Cu^+(NO)$ reflects the rapid O_2 desorption on the overexchanged catalyst, producing a high concentration of Cu^+ on the catalyst surface. As a result, the major adsorbate observed under conditions of the NO decomposition to N_2 and O_2 is $Cu^+(NO)$. Furthermore, the oxygen and nitrogen desorbed do not have to come from the same NO molecule. Indeed, a good fraction of oxygen desorbed came from the adsorbed oxygen of the Cu−ZSM-5 catalyst, as evidenced by $^{15}N^{18}O$ TPD and pulse NO reaction results in Figures 12 and 14. This oxygen is indicated as [O] in Figure 15. The sequence of formation of $Cu^+(NO)$, $Cu^{2+}O^-$, and $Cu^+O^-(NO)$ illustrated in the Figure 15 is similar to the sequence proposed by Aylor et al. in the reaction mechanism for NO decomposition over Cu−ZSM-5.[7] This mechanism suggests that $Cu^+(NO)$ adsorbs another NO molecule, forming $Cu^+(NO)_2$ species which in turn decomposes to $Cu^{2+}O^-$ and desorbs N_2O. Gaseous N_2O reacts with a Cu^+ site to desorb N_2. Although our TPR data suggest N_2O is an intermediate in the reaction, the present scheme (Figure 15) does not provide direct evidence to support the involvement of $Cu^+(NO)_2$ in the formation of N_2 or N_2O as proposed by a number of previous studies.[2−4,6,7]

Formation of part of O_2 goes through the route where bridged $Cu^{2+}(NO_3^-)$ is formed. Although the coordination capacity and site environment of Cu^{2+}, which is associated with the bridged nitrate, has not been determined, the correlation between IR intensity profile of bridged $Cu^{2+}(NO_3^-)$ and MS profiles of NO, O_2, and NO_2 suggest the following reaction. The bridged $Cu^{2+}(NO_3^-)$ serves as a precursor for the O−O bond formation.

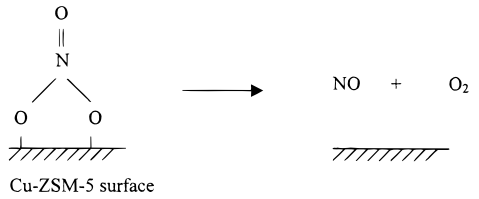

Conclusion

Comparison of FTIR spectra and MS rate profiles of the over- and underexchanged Cu−ZSM-5 catalysts shows that the overexchanged Cu−ZSM-5 (a) possessed more Cu^+ sites, (b) exhibited higher activity, and (c) generated Cu^+ sites at lower temperatures than underexchanged Cu−ZSM-5. Over- and underexchanged Cu−ZSM-5 produce similar adsorbates that differ in the rate of formation at different temperatures.

The step and pulse studies show that there is no correlation between the formation of N_2 and the $Cu^+(NO)_2$ species at 308 K, suggesting that the formation of N_2 from $Cu^+(NO)$ and $Cu^+(NO)_2$ is a complicated process. The N_2 formation accompanied by the presence of $Cu^+(NO)$ suggests that Cu^+ is most likely the site for initiating NO decomposition on the overexchanged Cu−ZSM-5. Formation of N_2 from NO adsorbed on the surface results in oxygen being left on the catalyst surface, changing the oxidation state of copper and aiding the formation of other adsorbate species. The sequence of adsorbate formation during the NO step and pulse switch is $Cu^+(NO)$, $Cu^+(NO)_2$, $Cu^{2+}(NO)$, $Cu^{2+}O^-(NO) > NO^+_{ad.} > Cu^{2+}(NO_3^-)$. Under NO decomposition conditions at 673 K, $Cu^+(NO)$ and $Cu^{2+}(NO_3^-)$ are the dominant adsorbates where the formation of $Cu^+(NO)$ prior to that of $Cu^{2+}(NO_3^-)$ further supports the beforementioned statement that Cu^+ initiates the NO decomposition reaction process. Although $Cu^{2+}(NO_3^-)$ decomposed to N_2, N_2O, NO_2, and O_2 during the TPD, it is not the sole precursor for the O_2 formation. $^{15}N^{18}O$ isotopic studies show the involvement of adsorbed oxygen on Cu−ZSM-5 in the O_2 formation during the pulse NO reaction.

Acknowledgment. Although the research described in this article has been funded wholly by the United States Environmental Protection Agency under assistance agreement R823529-01-0 to the University of Akron, it has not been subjected to the Agency's peer and administrative review and therefore may not necessarily reflect the views of the Agency and no official endorsement should be inferred.

References and Notes

(1) Iwamoto, M.; Hamada, H. *Catal. Today* **1991**, *10*, 57.
(2) Iwamoto, M.; Yahiro, H.; Mizuno, N.; Zhang, W.-X.; Mine, Y.; Furukawa, H.; Kagawa, S. *J. Phys. Chem.* **1992**, *96*, 9360.
(3) Giamello, E.; Murphy, D.; Magnacca, G.; Morterra, C.; Shioya, Y.; Nomura, T.; Anpo, M. *J. Catal.* **1992**, *136*, 510.
(4) Valyon, J.; Hall, W. K. *New Frontiers in Catalysis*; Proceedings of the 10th International Congress on Catalysis, 1992; Guczi, L., Solymosi, F., Tetenyi, P., Eds.; Akademiai Kiado: Budapest, Hungary, 1993; p 1341.
(5) Valyon, J.; Hall, W. K. *J. Phys. Chem.* **1993**, *97*, 7054.

(6) Spoto, G.; Zecchina, S.; Bordiga, S.; Ricchiardi, G.; Marta, G.; Leofanti, G.; Petrini, G. *Appl. Catal. B* **1994**, *3*, 151.
(7) Aylor, A. W.; Larsen, S. C.; Reimer, J. A.; Bell, A. T. *J. Catal.* **1995**, *157*, 592.
(8) Lei, G. D.; Adelman, B. J.; Sárkány, J.; Sachtler, W. M. H.; *Appl. Catal. B* **1995**, *5*, 245.
(9) Hoost, T. B.; Laframboise, K. A.; Otto, K. *Catal. Lett.* **1995**, *33*, 105.
(10) Wichterlová, B.; Dědeček, J.; Vondrová, A. *J. Phys. Chem.* **1995**, *99*, 1065.
(11) Hadjiivanov, K.; Klissurski, D.; Ramis, G.; Busca, G. *Appl. Catal. B* **1996**, *7*, 251.
(12) Cheung, T.; Bhargava, S. K.; Hobday, M.; Foger, K. *J. Catal.* **1996**, *158*, 301.
(13) Chen, H. Y.; Chen, L.; Lin, J.; Tan, K. L.; Li, J. *Inorg. Chem.* **1997**, *36*, 1417.
(14) Iwamoto, M.; Yoko, S.; Sakai, K.; Kagawa, S. *J. Chem. Soc., Faraday Trans. 1*. **1989**, *77*, 1629.
(15) Iwamoto, M.; Yahiro, H.; Tanda, K.; Mizuno, N.; Mine, Y.; Kagawa, S. *J. Phys. Chem.* **1991**, *95*, 3727.
(16) Li, Y.; Hall, W. K. *J. Catal.* **1991**, *129*, 202.
(17) Curtin, T.; Grange, P.; Delmon, B. *Catal. Today* **1997**, *36*, 57.
(18) Adelman, B. J.; Beutel, T.; Lei, G.-D.; Sachtler, W. M. H. *J. Catal.* **1996**, *158*, 327.
(19) Nakamoto, K. *Infrared and Raman Spectra of Inorganic and Coordination Compounds*, 3rd ed.; John Wiley & Sons: New York, 1978; p 295.
(20) Hadjiivanov, K.; Saussey, J.; Freysz, J. L.; Lavalley, J. C. *Catal. Lett.* **1998**, *52*, 103.
(21) Jang, H.-J.; Hall, W. K.; d'Itri, J. L. *J. Phys. Chem.* **1996**, *100*, 9416.
(22) Chuang, S. S. C.; Lopez, B. *Progress in Zeolite and Microporous Materials*; Studies in Surface Science and Catalysis 105; Chon, H., Ihm, S.-K., Uh, Y. S., Eds.; 1995; p 1477.
(23) Srinivas, G.; Chuang, S. S. C.; Debnath, S. *J. Catal.* **1994**, *148*, 748.
(24) Li, Y.; Hall, W. K. *J. Phys. Chem.* **1990**, *94*, 6145.
(25) McLafferty, F. W.; Stauffer, D. B. *The Wiley/NBS Registry of Mass Spectral Data*; John Wiley and Sons: New York, 1989; Vol. 1, p 3.
(26) Niemantsverdriet, J. W. *Spectroscopy in Catalysis*; VCH: New York, 1995; p 195.
(27) Chang, Y.-F.; McCarty, J. G. *J. Catal.* **1997**, *165*, 1.
(28) Richter-Addo, G. B.; Legzdins, P. *Metal Nitrosyls*; Oxford University Press: Oxford, 1992.
(29) Konduru, U. V. M.S. Thesis, The University of Akron, 1997.
(30) Trout, B. L.; Chakraborty, A. K.; Bell, A. T. *J. Phys. Chem.* **1996**, *100*, 17582.
(31) Wichterlová, B.; Dědeček, J.; Sobalík, Z.; Vondrová, A.; Klier, K. *J. Catal.* **1997**, *169*, 194.
(32) Konduru, M. V.; Chuang, S. S. C. Submitted for publication in *J. Catal.* **1999**.
(33) Konduru, M. V. Ph. D. Preliminary study, The University of Akron, 1999.